Anisotropy of Magnetic and Transport Properties of UAuSb$_2$ Single Crystals

R. Troć, Z. Bukowski*, J. Stępień-Damm

and C. Sułkowski

Institute of Low Temperature and Structure Research, Polish Academy of Sciences

P.O. Box 1410, 50-950 Wrocław 2, Poland

The uranium-gold diantimonide UAuSb$_2$ belongs to a numerous family of ternary compounds crystallizing in a tetragonal structure of the HfCuSi$_2$-type (space group $P4/nmm$). In this paper the results of magnetization, electrical resistivity and thermopower measured along the main crystallographic directions are reported. Two magnetic transitions, a ferromagnetic one at $T_C = 31$ K and probably an antiferromagnetic one at $T_N = 43$ K were found. The spontaneous magnetization at 1.9 K amounts about 0.8 μ_B for $B \parallel c$-axis. Electrical resistivity for $j \perp c$-axis exhibits a $T^2 \exp(-\Delta/kT)$ dependence at low temperatures and a Kondo effect at higher temperatures above T_N. The thermopower S for both main crystallographic directions shows a maximum at the temperature close to T_C and the lack of any anomaly at T_N.

PACS numbers: 71.20.Lp, 71.27.+a, 75.30.Gw

1. Introduction

The uranium-gold diantimonide UAuSb$_2$ belongs to a numerous family of ternary compounds crystallizing in a tetragonal structure of the HfCuSi$_2$-type (space group $P4/nmm$), which can be described as a filled USb$_2$ structure [1]. The de Haas–van Alfven (dHvA) experiments performed for this parent compound indicated the formation of the quasi-two-dimensional (QTD) electronic states, due to the layered character of this structure. It develops in the form of four kinds of nearly cylindrical Fermi surface pieces [2] for the magnetic field applied along the tetragonal [001] direction. In the case of UAuSb$_2$, planes of gold atoms intercalate into the unit cell of USb$_2$ increasing considerable the ratio c/a from 2.05 to 2.25. Previously there were reports on the magnetic and transport properties but made on polycrystalline samples of UAuSb$_2$ [3]. This compound was characterized as semimetallic Kondo lattice ferromagnet with $T_C = 36$ K. Magnetization experiment performed up to 4 T indicated the ordered moment to be about 1.3 μ_B, which presents a doubled value of the observed magnetization in the case of assuming a uniaxial magnetic anisotropy (i.e. the magnetization value is multiplied by 2). In the paramagnetic region the magnetic susceptibility followed a modified Curie–Weiss law due to a large bending of its temperature-dependent inverse form.

Recently, the electronic band structure of UAuSb$_2$ has been calculated by the full potential linear muffin-tin or-

bital (LMTO) method. Based on this calculation the obtained spectrum for the valence band was compared to the measured one by X-ray photoelectron spectroscopy (XPS) experiment [4]. A fairly good agreement was obtained. The cylindrical shape of the calculated Fermi surface as an indication of quasi-two dimensionality of the properties of UAuSb$_2$, related to its crystal structure, has also been presented.

2. Experimental details

Single crystals were grown by the self-flux method, as described in [5]. The starting elements with 3N — U, 5N — Au and Sb were taken with the appropriate ratio and an excess of a flux was used. They had the form of thin plates perpendicular to the c-axis with typical dimensions 3 mm × 3 mm × 1 mm. They had metallic luster and were stable in air for a long period of time. The obtained crystals were examined using a scanning electron microscope Philips 515 and their chemical composition was determined with an energy dispersive X-ray (EDX) spectrometer PV9800 using a standard procedure. For measurements single crystals were cut by a wire saw into bar-shaped specimens.

Integrated X-ray intensities were measured on a KM-4 four-circle diffractometer equipped with a CCD camera, using graphite-monochromated Mo K_α radiation ($\lambda = 0.71073$ Å).

Magnetic measurements were performed on oriented single crystals within the temperature range 1.9–400 K in magnetic fields up to 5 T employing a SQUID magnetometer. The electrical resistivity was measured over the temperature interval 4.2–300 K employing a standard

_____

* Present address: Laboratory for Solid State Physics, ETH Zürich, Switzerland.

dc four-point technique. The current leads were soldered with tin-lead alloy, while the voltage contacts were attached to the sample surface by spot-welding. Thermoelectric power measurements were carried out in the temperature range 5–300 K by a standard differential method with pure copper as a reference sample.

3. Results and discussion

3.1. Crystal structure

Table I summarizes the crystallographic details derived at room temperature. The corresponding atomic coordinates and displacement parameters are given in Table II. The interatomic distances are in turn listed in Table III. The occupancy factors were refined in a separate series of least-squares cycles, giving no significant deviation from the full occupancies for uranium and antimony, and a value for the Au occupancy at its site 2(a) is very close to 1.0 (see Table II). However, the displacement parameters for the Au atoms are almost double than those for the U and Sb atoms. In contrast to $UNi_{0.5}Sb_2$ [5], no superstructure has been detected.

TABLE I

Crystal data and structure refinement for $UAuSb_2$.

empirical formula	$AuSb_2U$
formula weight	678.50
temperature	293(2) K
wavelength	0.71073 Å
crystal system, space group	tetragonal, $P4/nmm$
unit cell dimensions	$a = 4.375(1)$ Å
	$c = 9.831(2)$ Å
volume	188.17(7) Å^3
Z, calculated density	2, 11.975 Mg/m^3
absorption coefficient	95.700 mm^{-1}
$F(000)$	564
θ range for data collection	11.43 to 39.36°
limiting indices	$-7 \leq h \leq 6$
	$-7 \leq k \leq 5$
	$-12 \leq l \leq 17$
reflections collected/unique	2606/357 [$R(\text{int}) = 0.0725$]
completeness to $\theta = 47.19°$	94.2%
refinement method	full-matrix least-squares on F^2
data/restraints/parameters	357/0/12
goodness-of-fit on F^2	1.096
final R indices [$I > 2\sigma(I)$]	$R1 = 0.0289$, $wR2 = 0.0644$
R indices (all data)	$R1 = 0.0329$, $wR2 = 0.0654$
extinction coefficient	0.0191(12)
largest diff. peak and hole	4.233 and –4.692 e Å^{-3}

TABLE II

Atomic coordinates, anisotropic and equivalent isotropic displacement parameters (Å$^2 \times 10^3$) for $UAuSb_2$. $U(\text{eq})$ is defined as one third of the trace of the orthogonalized U_{ij} tensor.

At.	Site	Occ.	x	y	z	U_{11}	U_{22}	U_{33}	$U(\text{eq})$
U	2c	1	1/4	1/4	0.2438(1)	7(1)	7(1)	7(1)	7(1)
Sb1	2a	0.998(5)	3/4	1/4	0	8(1)	8(1)	6(1)	7(1)
Sb2	2c	0.999(6)	1/4	1/4	0.6862(1)	7(1)	7(1)	16(1)	10(1)
Au	2b	0.926(4)	3/4	1/4	1/2	16(1)	16(1)	12(1)	15(1)

The anisotropic displacement factor exponent takes the form: $-2\pi^2[h^2a^{*2}U_{11} + \ldots + 2hka^*b^*U_{12}]$ $U_{23} = U_{12} = U_{13} = 0$. $U(\text{eq})$ is defined as one third of the trace of the orthogonalized U_{ij} tensor.

TABLE III

Selected interatomic distances [Å] for $UAuSb_2$.

U–Sb1	3.1691(7)	Au–Au	3.0936(7)
Sb2	3.2451(6)	Sb1	2.8527(8)
Au	3.3359(6)	Sb2–Sb2	3.0936(7)
U	4.375(1)		

3.2. Magnetic properties

In Fig. 1 we present the magnetization M (in units μ_B) measured for two options (zero field and field cooling) at $B = 0.1$ T along the easy magnetization c axis and also that perpendicular to this axis as a function of temperature. As seen, the two magnetic transitions can be inferred from these measurements, one at about 31 K of ferromagnetic character and that at 44 K probably of antiferromagnetic one. The inset to this figure displays the M vs. T curve determined also along the crystallographic direction perpendicular to the c axis but on enlarged scale. Magnetization curve taken at 1.9 K and shown in Fig. 1, reveals an almost rectangular partial hysteresis loop. The magnitude of the magnetic moment found at a magnetic field of 5 T, where the virgin magnetization is still far from saturation, is about 0.77 μ_B. This is considerably less than the moment reported in Ref. [3] (2×0.65 μ_B) from bulk measurements of this diantimonide. This demonstrates some preference of grains in the polycrystalline sample studied. It is also puzzled that the latter magnetization studies did not reveal the antiferromagnetic transition.

Figure 2 shows the temperature dependences of the magnetization M measured in magnetic fields up to 5 T for both main crystallographic axes a and c. In the inset to Fig. 1 we show the basal-plane magnetization vs. temperature on enlarged scale. As this figure demonstrates, the magnetization measured in the basal plane below the both ordered temperatures is considerably smaller than that along the c-axis. As seen, the character of both curves, i.e. along the easy and hard magnetization di-
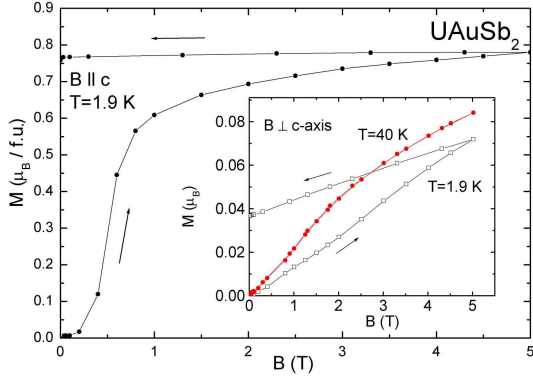
Fig. 1. Magnetization at 1.9 K for $B \parallel c$ and $B \perp c$ (inset).

rections, is very similar to each other, though the Curie temperature found from the inflection point of the magnetization curve of the latter direction is about 3 K lower than that determined for the easy direction. This is probably caused by very small magnetic response of the magnetization measured along the basal plane.
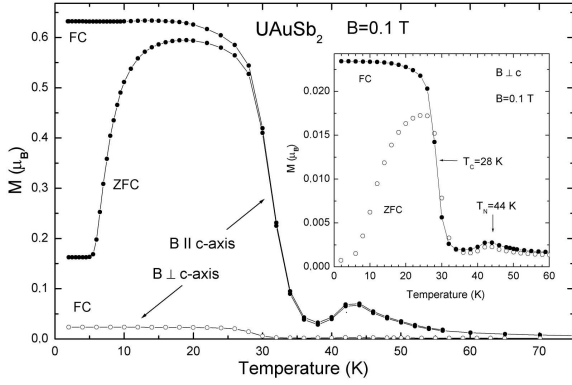
Fig. 2. Magnetization vs. temperature for $B \parallel c$ and $B \perp c$ (inset).

We have measured also a polycrystalline sample especially in the paramagnetic region because our single crystals were too small to get satisfied accuracy in such measurements. A large curvature of this dependence was obtained to which a modified Curie–Weiss (MCW) law has been fitted. The MCW parameters obtained in this work turned out to be very close to those previously reported for the polycrystalline sample in Ref. [3]. However, the χ^{-1} vs. T curve, reproduced from Fig. 2 of Ref. [3], has been erroneously presented.

3.3. Electrical resistivity

The temperature dependences of the electrical resistivity ρ for both directions in which $\boldsymbol{j} \perp c$-axis and $\boldsymbol{j} \parallel c$-axis are presented in Fig. 3 and in its inset, respectively. They are of similar temperature variation but have various magnitudes. For example, the values

at room temperature are 2.5 times larger for the latter direction with respect to the former one. We have analyzed in more detail the case where the current was flowed along a flat sample to which the c-axis was perpendicular to its surface. As Fig. 3 shows, in the low temperature region up to T_C the $\rho(T)$ variation can be fairly well fitted by the equation

$$\rho(T) = \rho_0 + aT^2 \exp(-\Delta/T),$$

where ρ_0 is the residual resistivity and the second term describes scattering of the conduction electrons on spin-wave excitations with the energy gap Δ in the spin-wave spectrum. We found $\Delta = 55$ K (see the corresponding parameters given in Fig. 3) which is comparable to that reported for the polycrystalline sample of 61 K [3].
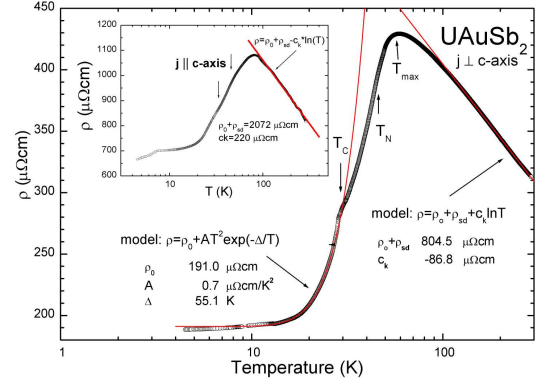
Fig. 3. Electrical resistivity vs. temperature for $\boldsymbol{j} \perp c$ and $\boldsymbol{j} \parallel c$ (inset).

The $\rho(T)$ curve at T_C (= 28 K) goes through a kink, and above this temperature this function still grows but not giving any visual anomaly at T_N. With further increasing temperature, but close around 60 K, this curve exhibits a broad peak and finally above 100 K, the resistivity in the whole paramagnetic region studied follows the standard Kondo formula: $\rho(T) = \rho_0 + \rho_{sd} - c_k \ln T$, where ρ_{sd} stands for the spin-disorder resistivity and c_k is the Kondo coefficient. The parameters occurring in the above two functions, found by least-squares fitting procedure, are given in the figure. We obtained the corresponding parameters larger than those given in Ref. [3]. As demonstrated in the inset of Fig. 3, the Kondo parameter c_k determined for $\boldsymbol{j} \parallel c$-axis is at least 3 times larger compared to that for $\boldsymbol{j} \perp c$-axis. However, due to the flat nature of the single crystals of UAuSb$_2$ and hence difficulties in precise measuring the resistivity along the c-axis, these data should be treated qualitatively.

Recently, Coqblin [6] has presented a review with a special emphasis on the underscreened Kondo effect in ferromagnetic-Kondo competition in several cerium, ytterbium and uranium compounds. Thus for this group of such compounds also systems UT$_{1-x}$Sb$_2$ (T = Ni, Co, Cu) have been included. It seems that we have to add to this group also UAuSb$_2$, despite the antiferromagnetic behavior of this compound between 31–44 K.

3.4. Thermopower

The temperature dependences of the thermopower (TEP) measured along the main axes are shown in Fig. 4. As usually in such type of compounds, the TEP of
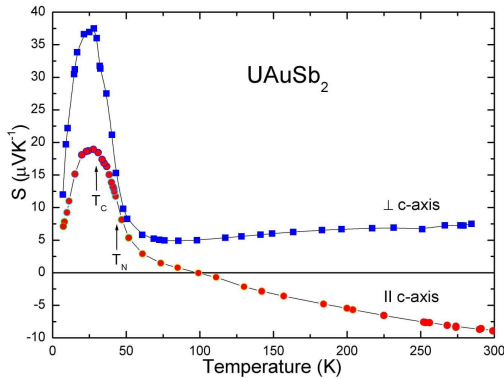
Fig. 4. Thermopower vs. temperature for $S \parallel c$ and $S \perp c$.

UAuSb$_2$ is highly anisotropic. The TEP along the tetragonal c-axis is negative at temperatures above 100 K, and its absolute value $S_\parallel$ increases with increasing temperature. After changing its sign at 100 K it becomes positive. Next, in the vicinity of T_N, where the maximum slope is reached together with that along the a-axis, both these curves increase further and they go through maxima at a few temperatures below T_C, but with different values of $S_\parallel$ and $S_\perp$ at $T_{max} = 25$ K, namely 20

and 37 mV/K, respectively. After passing through their maxima, these two curves decrease almost linearly and by extrapolation they achieve $S_i = 0$ at $T = 0$ K. In contrary to $S_\parallel(T)$, the $S_\perp(T)$ curve is positive in the whole temperature range studied. Almost the same overall behavior was found in the case of UCuSb$_2$ [7], though the latter compound is only a ferromagnet below 113 K. The significant anisotropy in $S_i(T)$ over the whole temperature range studied is likely associated with anisotropic Fermi surface. Considering the similarity in $S_i(T)$ of both Cu- and Au-diantimonides one can suggest that the peak structure in $S_i(T)$ observed in these two compounds is probably of the phonon drag origin, despite the coincidence with T_C for the latter compound.

References

[1] M. Brylak, M.H. Möller, W. Jeitschko, *Solid State Chem.* **115**, 305 (1995).

[2] D. Aoki, P. Wiśniewski, K. Miyake, N. Watanabe, R. Settai, E. Yamamoto, Y. Haga, Y. Onuki, *J. Phys. Soc. Jpn.* **68**, 2182 (1999).

[3] D. Kaczorowski, R. Kruk, J.P. Sanchez, B. Malaman, F. Wastin, *Phys. Rev. B* **58**, 9227 (1998).

[4] J.A. Morkowski, A. Szajek, E. Talik, R. Troć, *J. Alloys Comp.* **443**, 20 (2007).

[5] Z. Bukowski, D. Kaczorowski, J. Stępień-Damm, D. Badurski, R. Troć, *Intermetallics* **12**, 138 (2004).

[6] B. Coqblin, *Acta Phys. Pol. A* **113**, 39 (2008) and references therein.

[7] Z. Bukowski, R. Troć, J. Stępień-Damm, C. Sułkowski, V.H. Tran, *J. Alloys Comp.* **403**, 65 (2005).